# Structural phase transition in deuterated benzil $C_{14}D_{10}O_2$: Neutron inelastic scattering

D. J. Goossens* and T. R. Welberry
*Research School of Chemistry, The Australian National University, Canberra 0200, Australia*

M. E. Hagen
*Spallation Neutron Source, Oak Ridge National Laboratory, P.O. Box 2008, Tennessee 37831, USA*

J. A. Fernandez-Baca
*Center for Neutron Scattering, Oak Ridge National Laboratory, P.O. Box 2008, Tennessee 37831, USA*
(Received 9 January 2006; published 26 April 2006)

Neutron inelastic scattering has been used to examine the structural phase transition in deuterated benzil $C_{14}D_{10}O_2$. The transition in benzil, in which the unit cell goes from a trigonal $P3_121$ unit cell above $T_C$ to a cell doubled $P2_1$ unit cell below $T_C$, leads to the emergence of a Bragg peak at the $M$-point of the high temperature Brillouin zone. It has previously been suggested that the softening of a transverse optic phonon at the $\Gamma$-point leads to the triggering of an instability at the $M$-point causing the transition to occur. This suggestion has been investigated by measuring the phonon spectrum at the $M$-point for a range of temperatures above $T_C$ and the phonon dispersion relation along the $\Gamma$-$M$ direction just above $T_C$. It is found that the transverse acoustic phonon at the $M$-point is of lower energy than the $\Gamma$-point optic mode and has a softening with temperature as $T$ approaches $T_C$ from above that is much faster than that of the $\Gamma$-point optic mode. This behavior is inconsistent with the view that the $\Gamma$-point mode is responsible for triggering the phase transition. Rather the structural phase transition in benzil appears to be driven by a conventional soft TA mode at the $M$-point.

DOI: 10.1103/PhysRevB.73.134116 PACS number(s): 68.35.Rh, 63.20.Dj, 61.12.−q

## I. INTRODUCTION

Benzil (diphenylethanedione, $C_6H_5$-CO-CO-$C_6H_5$, see Fig. 1) forms an organic molecular crystal with a structure analogous to $\alpha$-quartz, space group $P3_121$ at room temperature.[1] Indeed it shows electric, elastic, and optical properties analogous to quartz and is sometimes referred to as "organic quartz" (see, for example, Ref. 2). As such it is an archetypal system which has undergone much study over many years (early Raman studies include Refs. 3–6)—although, somewhat surprisingly, no neutron inelastic scattering (NIS) study has previously been reported.

Benzil shows numerous interesting physical properties including nonlinear optical properties[7] and a ferroelectric/ferroelastic first order phase transition at $T_C \sim 83.5$ K. The low temperature phase is monoclinic, $P2_1$; it has been described[8] as a "monoclinic base-centered $C$-type Bravais lattice whose primitive cell is triclinic." The difference in the molecular structure of benzil in the high and low temperature phases is shown in Fig. 5 of Ref. 1. The phase transition was observed through the appearance of birefringent properties below $T_C$,[9] and has since been observed using a variety of techniques: Raman,[10–14] Brillouin light scattering,[8,15] infrared,[16] heat capacity,[17] dielectric spectra,[18] thermal expansion,[19] and dielectric constant measurements.[20] The phase transition appears to be weakly first order.

The crystal structures in the two phases have been well determined using x-rays,[1] and it has been shown[21] that the room temperature structures of $C_{14}H_{10}O_2$ (referred to as h-benzil) and $C_{14}D_{10}O_2$ (d-benzil) are virtually identical, the only difference being the influence of the mass difference on the atomic displacement parameters. Further, there is no evidence for deuteration changing the nature of the phase transition.[20]

The Raman scattering[10–14] and infrared absorption[16] measurements have characterized the softening of a zone center ($\Gamma$-point) transverse optic mode of $E$ symmetry on approaching $T_C$ from above. This mode does not soften to zero energy but saturates at $\sim 1$ meV at $T_C$ and then splits in the low symmetry phase and hardens as the temperature is lowered further. Based on these observations it has been suggested by Tolédano[22] that the transition is driven by the softening of this $\Gamma$-point mode which then triggers an instability at the $M$-point of the zone boundary [the $M$-point lies at $(0\ \frac{1}{2}\ 0)$ in the reciprocal cell]. This argument was seemingly supported by the observation of x-ray diffuse scattering,[23] around both the $\Gamma$-point and $M$-point with the $\Gamma$-point diffuse scattering more divergent as $T_C$ was approached.

However, in order to directly test the validity of this hypothesis, it is necessary to measure the temperature dependence of the $M$-point soft mode as well as the zone center mode. In this paper we report such a measurement, using NIS. The advantage of NIS measurements for determining phonon modes is the ability of NIS to measure these modes at any point in the Brillouin zone.

## II. EXPERIMENT

The NIS measurements reported in this paper were carried out at the High Flux Isotope Reactor, Oak Ridge National Laboratory, using the HB1 triple axis spectrometer (TAS). For this work HB1 was operated with highly oriented pyrolytic graphite monochromator and analyzer crystals, utilizing

 

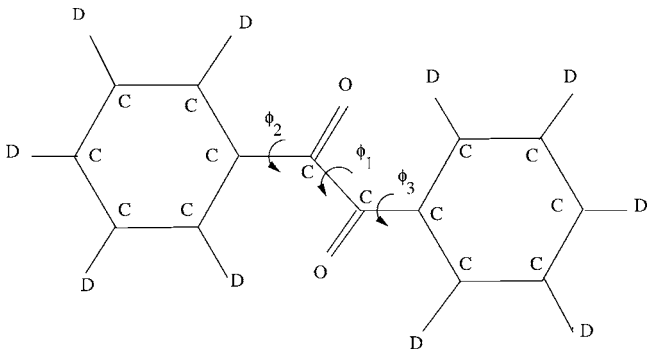


FIG. 1. Schematic diagram of the benzil molecule. $\phi_i$ are the internal degrees of freedom.

the (002) reflection planes to scatter the beam. A fixed final energy of $E_F=14.7$ meV was used throughout the measurements which allowed for the use of a pyrolytic graphite filter in the scattered beam in order to reduce the amount of $\lambda/2$ contamination (see, Ref. 24). The Soller collimation employed was 48′ of arc before the monochromator, 20′ between monochromator and sample, and again between sample and analyzer, and 48′ between the analyzer and detector. This combination of collimation and fixed analyzing energy led to an energy resolution of 0.49 meV FWHM as measured using the incoherent elastic scattering from a standard vanadium rod sample.

The sample used was a single crystal of d-benzil with dimensions of 16 mm $\times$ 8 mm $\times$ 6 mm where the long axis was, to a close approximation, the hexagonal $c$ axis. In this paper we use a hexagonal unit cell notation for benzil with lattice parameters at room temperatures of $a=8.376$ Å and $c=13.70$ Å. The sample was mounted with its $c$-axis vertical inside a sealed sample can containing helium as an exchange gas. This can was attached to the copper block of a closed cycle refrigerator that was in turn mounted on the sample table of the HB1 TAS. As a consequence the horizontal scattering plane of the HB1 TAS allowed us to perform measurements at wave vectors in the $(h,k,0)$ plane in reciprocal space.

The closed cycle refrigerator allowed us to control the temperature of the sample between room temperature and 90 K. It should be noted that the transition temperature of d-benzil is 88.1 K and that, since the transition is first order, the crystal could not reversably be driven through the phase transition. For the measurements reported in this paper the temperatures were stable to ±0.06 K.

## III. RESULTS

The principal aim of this work has been to examine the temperature dependence of the lowest energy (TA) phonon in d-benzil at the $M$-point of the high temperature Brillouin zone. Since the 88.1 K (Ref. 20) structural phase transition in d-benzil (and the equivalent 83.5 K transition in h-benzil) leads to the appearance of a Bragg peak at the $M$-point it seems reasonable to expect the $M$-point TA mode to show softening as a function of temperature on approaching $T_C$. In order to characterize this softening we have performed

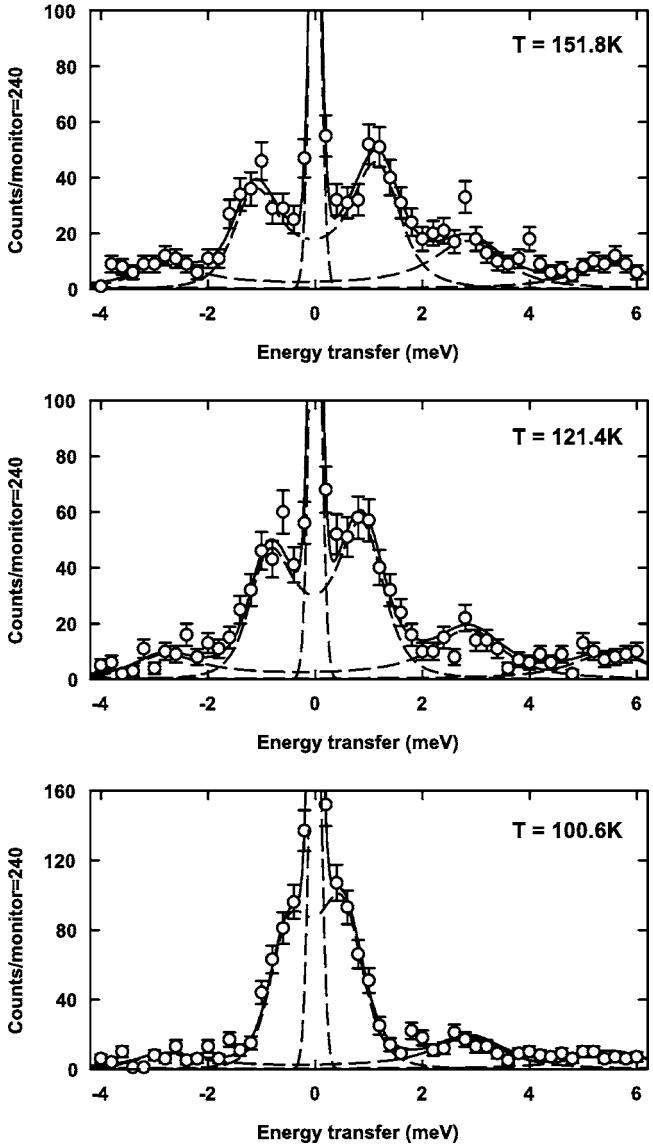


FIG. 2. Fit of Eq. (2), allowing for instrument resolution and temperature factors, to the excitation spectrum of $C_{14}D_{10}O_2$ at the $Q=(4,-0.5,0)$ $M$-point for temperatures of 151.8, 121.4, and 100.6 K. Hollow circles give data points, dashed lines give examples of fits to (pairs of) excitation peaks, and the solid lines show the resulting envelopes.

constant-$Q$ inelastic measurements at the $(4,-0.5,0)$ $M$-point at various temperatures from 93 to 152 K. Measurements were restricted to the range $T>90$ K.

A complete set of the low energy phonon dispersion relations were surveyed along the $[4,-\xi,0]$ $\Gamma$-$M$ direction from $(4,0,0)$ $\Gamma$ to $(4,-0.5,0)$ $M$ at 100 K. Within the $l=0$ plane the reciprocal space of benzil has sixfold symmetry, for example, directions such as $[4+\xi,-\xi,0]$ are equivalent to $[4,-\xi,0]$. However, for planes with $l\neq 0$ the true threefold symmetry of benzil becomes apparent and it is the $[4,-\xi,l\neq 0]$ direction that remains as a symmetry direction. It should be noted that in the x-ray diffuse scattering measurements a strong line of diffuse scattering is seen along $[4,-\xi,0]$ while the line along $[4+\xi,-\xi,0]$ is weak.[25,26]

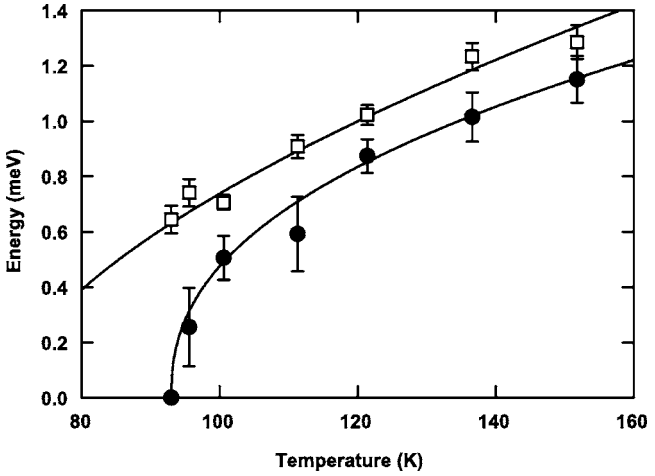


FIG. 3. The temperature dependence of the TA phonon energy ($\Omega_{TA}$, □) and the energy at which the DHO function peaks ($\Omega_P$, ●) [see Eqs. (2) and (3)] at the $(4,-0.5,0)$ $M$-point. The solid lines are guides for the eye.

Figure 2 shows the measured spectra at the $(4,-0.5,0)$ $M$-point for temperatures of 151.8, 121.4, and 100.6 K. These measured phonons in d-benzil show significant line shape broadening and as a consequence we have fitted each of the measured spectra to a line shape function, convoluted with the instrumental resolution function for the triple axis spectrometer.

The form we have used to model the broadened phonon line shape is the damped harmonic oscillator (DHO) function (see, for example, Section III of Appendix B of Ref. 27). This line shape has been widely used to model damped excitations, some examples being, the soft phonons in $SrTiO_3$ (Ref. 28) and $LaAlO_3$,[29] the spin waves in USb,[30] $Rb_2Mn_xMg_{1-x}F_4$,[31] and $La_{1.725}Sr_{0.275}NiO_4$,[32] and the roton in $^4$He.[33] For a single phonon the dynamic structure factor $S(Q,E)$ for NIS can be written in the form

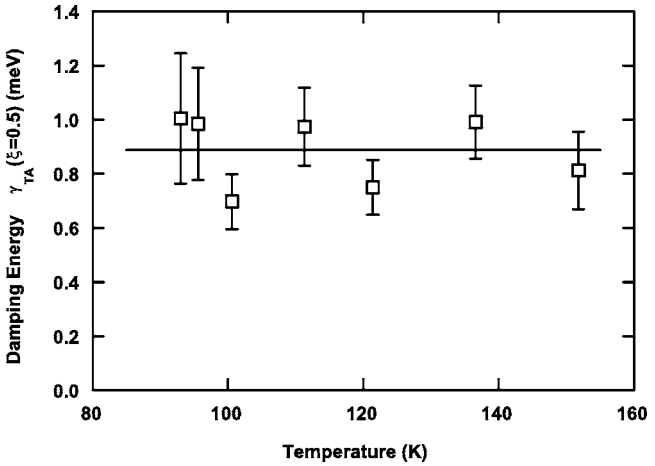


FIG. 4. The phonon damping for the TA phonon at the $M$-point, $\gamma_{TA}$ [see Eq. (2)] as a function of $T$. The solid line is a guide for the eye, demonstrating the constant value of $\gamma_{TA}$.

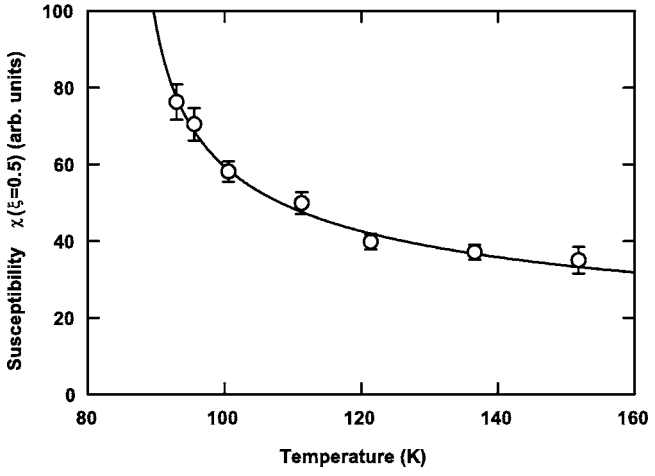


FIG. 5. The amplitude $\chi(Q)$ [see Eq. (1)] for the $M$-point TA phonon as determined from the fits. The solid line is a fit to Eq. (8).

$$S(Q,E) = \left(\frac{E}{k_B T}\right)\left[1 - \exp\left(\frac{-E}{k_B T}\right)\right]^{-1} \chi(Q) F(Q,E), \quad (1)$$

where $\chi(Q)$ is the amplitude (isothermal susceptibility) and $F(Q,E)$ is the spectral weight function. For the DHO line shape the spectral weight function is given by

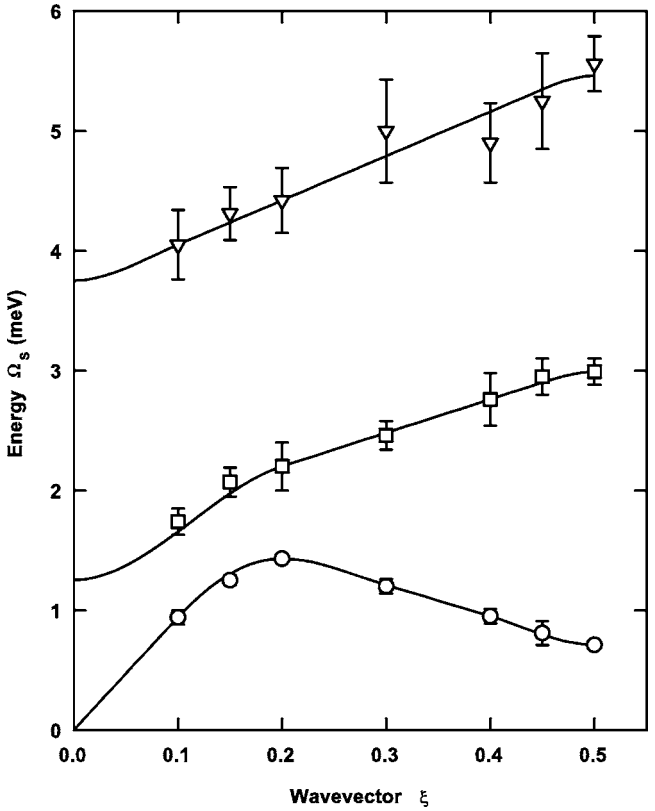


FIG. 6. Observed phonon dispersion curves for d-benzil ($C_{14}D_{10}O_2$) along the direction $[4,-\xi,0]$ at 100 K. The phonon energies $\Omega_S$ are derived from fits of Eq. (2) to the measured spectra at this temperature. ○ gives the TA mode, □ the $TO_1$, and ▼ the $TO_2$.

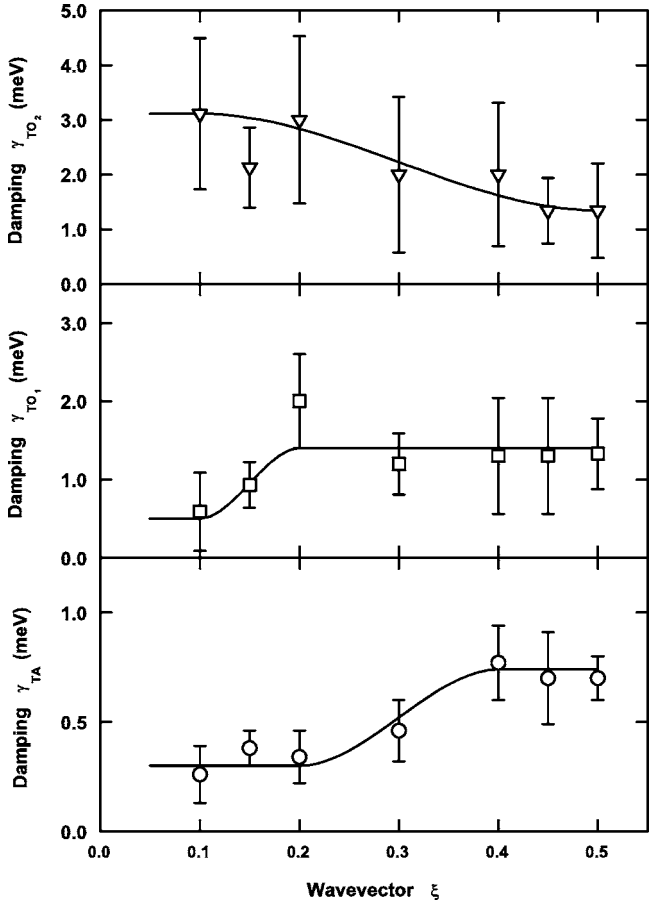


FIG. 7. Damping, [$\gamma_S$ in Eq. (2)] for the transverse phonon modes (plotted in Fig. 6) as a function of the wave vector $[4,-\xi,0]$ at 100 K. Plotted with symbols as in Fig. 6.

$$F(Q,E) = \frac{1}{\pi}\left(\frac{\gamma_S(Q)\Omega_S^2(Q)}{[E^2-\Omega_S^2(Q)]^2+[\gamma_S(Q)E]^2}\right), \qquad (2)$$

where $\Omega_S(Q)$ is the "pole" energy (phonon energy when the damping is small) and $\gamma_S(Q)$ is the damping. In the limit that $\gamma_S(Q)\to 0$ this line shape reduces to a sharp peak $[\delta(E-\Omega_S(Q))]$ at the "phonon energy" $\Omega_S(Q)$.

The instrumental resolution function used in the convolution was determined using the RESTRAX program[34] with the appropriate instrumental parameters for the HB1 TAS given in Sec. II and a sample mosaic spread of 0.4°. In Fig. 2 the solid line is the envelope resulting from fitting three DHO functions, convoluted with the resolution function, to the inelastic spectrum—individual peak fits are noted with dashed lines. Also included is a Gaussian "elastic line" peak to account for $\lambda/2$ contamination from the $(8,-1,0)$ Bragg peak. Even though a pyrolytic graphite filter was used in front of the sample to analyzer collimator to reduce the $\lambda/2$ contamination a small residual amount remains apparent.

The three DHO functions used to model the phonon spectrum account for the TA mode, which is at lowest energy, and then two optic phonons, $TO_1$ and $TO_2$, at higher energy. It should be noted that the symmetric form of the DHO in Eq. (2) constrains equivalent phonon peaks on energy loss and gains to have the same values for $\chi_S(Q)$, $\Omega_S(Q)$, and $\gamma_S(Q)$. The difference in peak heights and widths between energy loss and gain is solely given by the thermal population factor in Eq. (2) and the resolution function. Furthermore the two optic phonons $TO_1$ and $TO_2$ at the $M$-point show no measurable temperature dependence. As a consequence we have determined the parameters $\chi_{TO_1}$, $\Omega_{TO_1}$, $\gamma_{TO_1}$, $\chi_{TO_2}$, $\Omega_{TO_2}$, and $\gamma_{TO_2}$ at 151.8 K and held them fixed at all other temperatures. This means that the only variable parameters to fit the spectra at temperatures $T<151.8$ K are the three parameters $\chi_{TA}$, $\Omega_{TA}$, and $\gamma_{TA}$, describing the soft TA mode.

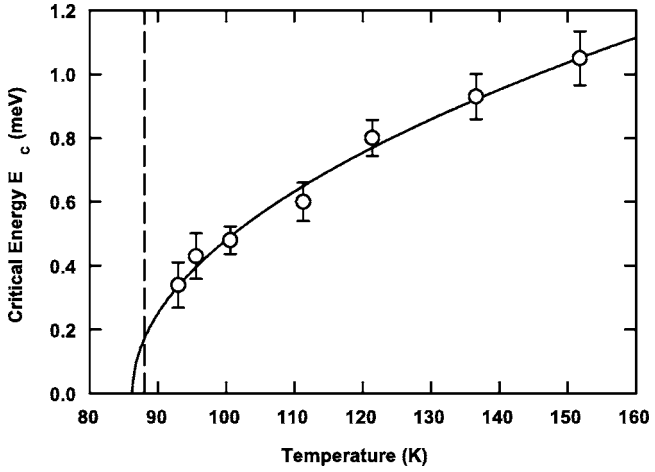


FIG. 8. Critical energy width $E_C$ [Eq. (5)] as a function of $T$; the solid line is a fit to Eq. (7). The dashed line shows the transition temperature $T_C$ from bulk measurements (Ref. 20).

The temperature dependence of the values of $\Omega_S(Q)$ and $\gamma_S(Q)$ for the TA phonon [$\Omega_{TA}(Q)$ and $\gamma_{TA}(Q)$, respectively] at the $M$-point are shown in Figs. 3 and 4, respectively. It is interesting to note that $\gamma_S(Q)$ for this $M$-point TA mode is essentially independent of temperature, the flat solid line shown in Fig. 4 is the average value of the data points, indicating a constant (temperature independent) damping mechanism. In $SrTiO_3$ (Ref. 28) and $LaAlO_3$ (Ref. 29) it is also observed that, for temperatures just above $T_C$, the damping constant for the soft phonon is independent of temperature.

It should be noted that when $\gamma_S(Q)\neq 0$ the energy at which the DHO function peaks is *not* the phonon energy $\Omega_S(Q)$ but instead the peak energy $\Omega_P(Q)$ which is given by

$$\Omega_P(Q) = \sqrt{\Omega_S^2(Q) - \tfrac{1}{2}\gamma_S^2(Q)}. \qquad (3)$$

Also shown in Fig. 3 are the values for $\Omega_P(Q)$ calculated from Eq. (3). At 93 K (the lowest measurement temperature in Fig. 3) the argument of the square root in Eq. (3) is negative indicating that the phonon is overdamped (i.e., there is only a single peak at zero energy), and as a consequence we have taken $\Omega_P(Q)=0$ for this data point. Figure 5 shows the temperature dependence of the amplitude $\chi(Q)$ [see Eq. (1)] for the $M$-point phonon as determined from the fits.

To determine the phonon dispersion relations at 100 K along the $[4,-\xi,0]$ direction a series of constant-$Q$ inelastic scans was performed for different values of $\xi$. These scans were each fitted to a series of DHO functions in the same

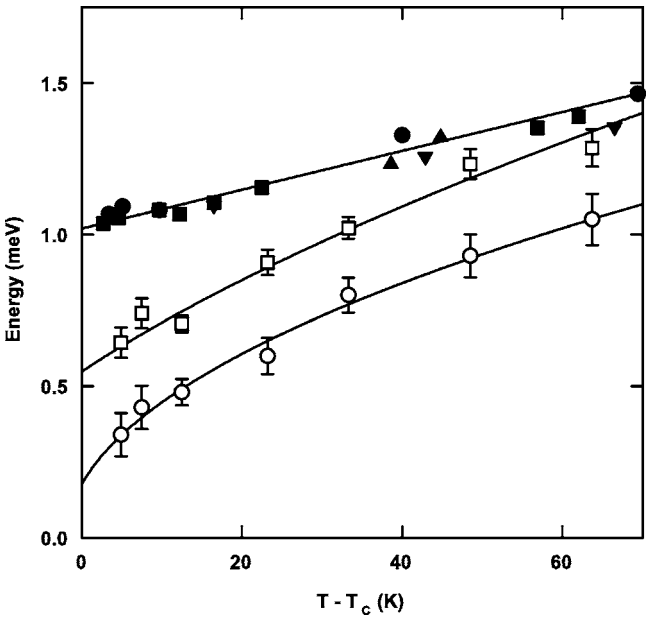


FIG. 9. $\Omega_{TA}$ and $E_C$ for the $M$-point TA mode (from this work), plotted on the same scale as the results for the $E$ mode at $\Gamma$ from the literature. □ and ○ refer to $\Omega_{TA}$ and $E_C$ from this work. ● relates to Ref. 12, ■ to Ref. 13, ▲ to Ref. 18, and ▼ to Ref. 41.

way that the scans at the $(4,-0.5,0)$ $M$-point were fitted. In Fig. 6 the phonon dispersion relations determined at 100 K along the $[4,-\xi,0]$ direction are shown by the open symbols.

The dispersion relations in Fig. 6 were defined by plotting the results for $\Omega_S(Q)$ and the corresponding results for $\gamma_S(Q)$ at 100 K are plotted in Fig. 7. It is, however, the case that for the values of $\Omega_S(Q)$ and $\gamma_S(Q)$ plotted in Figs. 6 and 7, respectively, there is not a substantial difference between $\Omega_S(Q)$ and $\Omega_P(Q)$ except for the TA mode at the $M$-point $(4,-0.5,0)$.

## IV. DISCUSSION

The results summarized in Figs. 2 and 3 clearly indicate that the $M$-point TA phonon is softening with decreasing temperature as $T_C$ is approached. However, from the perspective of the theory of critical phenomena neither $\Omega_{TA}(Q)$ nor $\Omega_P(Q)$, nor for that matter $\gamma_{TA}(Q)$, is a good measure of the "critical narrowing" of the characteristic (critical) energy width $E_C$ on approaching the structural phase transition. A very useful definition of the characteristic energy width $E_C$ for the critical scattering is given in Chap. 7 of Ref. 35 through the spectral weight function $F(Q,E)$. The spectral weight function is, in its definition, required to obey the normalization condition

$$\int_{-\infty}^{\infty} F(Q,E)dE = 1 \tag{4}$$

and the characteristic (critical) energy, $E_C$, is then defined[35] by the relation

$$\int_{-E_C}^{E_C} F(Q,E)dE = \tfrac{1}{2}. \tag{5}$$

The $F(Q,E)$ for the DHO given in Eq. (2) satisfies the normalization condition given in Eq. (4). Hence, we have determined values for the characteristic energy $E_C$ at each temperature by using the values of $\Omega_{TA}(Q)$ and $\gamma_{TA}(Q)$ from the fits at each temperature and numerically integrating the left-hand side of Eq. (5), where $F(Q,E)$ is the spectral weight function for the TA mode, until we reach a limit that satisfies Eq. (5). These values for $E_C$ are plotted as a function of temperature in Fig. 8. The error bars given for $E_C$ in Fig. 8 were found using the standard relation

$$\delta E_C = \sqrt{\left(\frac{\partial E_C}{\partial \Omega_{TA}}\delta\Omega_{TA}\right)^2 + \left(\frac{\partial E_C}{\partial \gamma_{TA}}\delta\gamma_{TA}\right)^2} \tag{6}$$

and the appropriate numerical evaluation of the derivatives.

As might be expected the values of $E_C$ plotted in Fig. 8 decrease (i.e., show a narrowing) with decreasing temperature. We have fitted the values of $E_C$ to a power law temperature dependence given by

$$E_C(T) = E_0 t^x = E_0 \left|\frac{T - T_C^*}{T_C^*}\right|^x, \tag{7}$$

where $x$ is the critical exponent and $T_C^*$ is the "critical" temperature. In these fits the critical exponent is fixed at the classical (mean field) value $x=0.5$. It is worth noting that in the case of strontium titanate ($SrTiO_3$), the prototypical example of a displacive structural phase transition, the $R$-point soft phonon follows such a form ($E_C^2 \propto T - T_C$) over a wide range of reduced temperature above $T_C$.[36–38] The solid line in Fig. 8 is a best fit result with $x=0.5$ fixed and corresponds to the values $T_C^*=(86.3\pm2.3)$ K and $E_0=(1.21\pm0.08)$ meV.

The power law form of Eq. (7) is a characteristic form for second order (continuous) phase transitions while it is known from bulk measurements that the phase transition in d-benzil and h-benzil is weakly first order.[20] It is, therefore, not surprising that the critical temperature $T_C^*=(86.3\pm2.3)$ K is lower than the true phase transition temperature for d-benzil of 88.1 K.[20] This behavior is observed at other first order phase transitions, for example, the antiferromagnetic phase transition in $UO_2$. Neutron scattering measurements of both the inverse correlation length ($\kappa$) (Ref. 39) and the critical energy width ($E_C$) (Ref. 40) for $UO_2$ show a power law behavior that extrapolates to a $T_C^* \sim 25$ K some 7 K below the true (first order) transition temperature of 31.7 K.[40]

A similar behavior can also be seen in the temperature dependence of the amplitude (susceptibility) $\chi(Q)$ which was plotted in Fig. 5. Again we can fit this to the characteristic second order form

$$\chi(Q,T) = \chi_0(Q)t^{-\gamma} = \chi_0(Q)\left|\frac{T - T_C^*}{T_C^*}\right|^{-\gamma}. \tag{8}$$

However in this case a good fit cannot be obtained by fixing $\gamma$ at its classical (mean field) value of 1.0, and instead

we must let all three parameters vary. The best fit result, which is shown by the solid line in Fig. 5, has the values $\gamma=0.37\pm0.10$, $T_C^*=(86.2\pm4.5)$ K, and $\chi_0(Q)=30.0\pm1.5$. The value for $T_C^*=(86.2\pm4.5)$ K is very close to the value obtained from the fit to $E_C(T)$ of $T_C^*=(86.3\pm2.3)$ K.

A comparison of the $M$-point mode we have observed with the $\Gamma$-point mode observed in previous studies is shown in Fig. 9. This figure shows, by the solid data points, the energies reported in the literature[12,13,18,41] for the $\Gamma$-point $TO_1$ mode (which is also known as the $E$ mode in the Raman scattering papers) as a function of the temperature above the transition temperature, i.e., $T-T_C$. On the same scale we have plotted the phonon energy $\Omega_{TA}$ (open circles) and critical energy $E_C$ (open squares) for the $M$-point TA mode. Figure 9 shows that at all temperatures the TA mode at the $M$-point is of lower energy than the $TO_1$ (a.k.a the $E$ mode) at the $\Gamma$-point and that as $T_C$ is approached from above the TA mode softens more rapidly, both in proportional and absolute terms. This strongly suggests that, contrary to the earlier suggestion,[22] the softening of the $\Gamma$-point mode is unlikely to be the primary mechanism driving the zone-boundary softening that leads to the cell doubling at the phase transition. It is possible that the order parameter coupling posited in (Ref. 22) does contribute to the transition but it does not trigger an instability at the $M$-point; rather, the instability is intrinsically present.

## V. CONCLUSIONS

The suggestion that the 88.1 K phase transition in deuterated benzil (83.5 K in benzil) occurs because of the softening of a $\Gamma$-point transverse optic phonon that triggers an instability at the $M$-point[22] has been tested by neutron inelastic scattering. An examination of the temperature dependence of the transverse acoustic phonon at the $M$-point shows that it has an energy that is always lower than that of the $\Gamma$-point optic mode and that it softens more rapidly than the $\Gamma$-point mode as the transition temperature is approached. The behavior of the $M$-point phonon is consistent with that of a conventional soft mode; such transitions are not the norm in organic molecular systems, but neither are they unprecedented.[42,43] As a consequence we conclude that there is no evidence that the phase transition is driven, or triggered, by the $\Gamma$-point optic phonon.

## ACKNOWLEDGMENTS

D.J.G. and T.R.W. thank A.P. Heerdegen for technical support and the Australian Research Council and Access to Major Research Facilities Program for financial support. Oak Ridge National Laboratory is managed by UT-Battelle, LLC for the U.S. Department of Energy under Contract No. DE-AC05-00OR22725.

*Electronic address: goossens@rsc.anu.edu.au

[1] M. More, G. Odou, and J. Lefebvre, Acta Crystallogr., Sect. B: Struct. Sci. **43**, 398 (1987).
[2] T. M. Kolev and B. A. Stamboliyska, Spectrochim. Acta, Part A **58**, 3127 (2002).
[3] S. A. Solin and A. K. Ramdas, Phys. Rev. **174**, 1069 (1968).
[4] F. Stenman, J. Chem. Phys. **51**, 3141 (1969).
[5] H. Claus, H. H. Hacker, H. W. Schrötter, J. Brandmüller, and D. Hassühl, Phys. Rev. **187**, 1128 (1969).
[6] H. Claus, H. W. Schrötter, and J. Brandmüller, J. Chem. Phys. **52**, 6448 (1970).
[7] J. Jerphagon, IEEE J. Quantum Electron. **QE-7**, 42 (1971).
[8] R. Vacher, M. Boissier, and J. Sapriel, Phys. Rev. B **23**, 215 (1981).
[9] P. H. Esherick and B. E. Kohler, J. Chem. Phys. **59**, 6681 (1973).
[10] P. Figuiére and H. Szwarc, Mol. Cryst. Liq. Cryst. **32**, 27 (1976).
[11] P. Figuiére and H. Szwarc, Mol. Cryst. Liq. Cryst. **35**, 1 (1976).
[12] D. R. Moore, V. J. Tekippe, A. K. Ramdas, and J. C. Tolédano, Phys. Rev. B **27**, 7676 (1983).
[13] J. Sapriel, A. Boudou, and A. Perigaud, Phys. Rev. B **19**, 1484 (1979).
[14] L. Colombo, D. Kirin, V. Volovsek, N. E. Lindsay, J. F. Sullivan, and J. R. Durig, J. Phys. Chem. **93**, 6290 (1989).
[15] A. Yoshihara, E. R. Bernstein, and J. C. Raich, J. Chem. Phys. **79**, 2504 (1983).
[16] A. L. Roy, O. Et-Tabti, and R. Guérin, J. Mol. Struct. **294**, 147 (1993).
[17] A. Dworkin and A. H. Fuchs, J. Chem. Phys. **67**, 1789 (1977).
[18] J. Petzelt, Y. G. Goncharov, G. V. Kozlov, A. A. Volkov, B. Wyncke, and F. Brehat, Czech. J. Phys., Sect. B **34**, 887 (1984).
[19] D. Havlik, W. Schranz, H. Warhanek, P. Zielinski, M. More, and G. Odou, Ferroelectrics **190**, 95 (1997).
[20] D. J. Goossens, X. Wu, and M. Prior, Solid State Commun. **136**, 543 (2005).
[21] R. O. Piltz and W. T. Klooster (private communication) (2004).
[22] J. C. Tolédano, Phys. Rev. B **20**, 1147 (1979).
[23] H. Terauchi, T. Kojima, K. Sakaue, F. Tajiri, and H. Maeda, J. Chem. Phys. **76**, 612 (1982).
[24] S. M. Shapiro and N. J. Chesser, Nucl. Instrum. Methods **101**, 183 (1972).
[25] T. R. Welberry, D. J. Goossens, A. J. Edwards, and W. I. F. David, Acta Crystallogr., Sect. A: Found. Crystallogr. **A57**, 101 (2001).
[26] T. R. Welberry, D. J. Goossens, W. I. F. David, M. J. Gutmann, M. J. Bull, and A. P. Heerdegen, J. Appl. Crystallogr. **36**, 1440 (2003).
[27] S. W. Lovesey, *Theory of Neutron Scattering from Condensed Matter* (OUP, UK, 1984), Vol. 1.
[28] S. M. Shapiro, J. D. Axe, G. Shirane, and T. Riste, Phys. Rev. B **6**, 4332 (1972).
[29] J. K. Kjems, G. Shirane, K. A. Muller, and H. J. Scheel, Phys. Rev. B **8**, 1119 (1973).
[30] M. Hagen, W. G. Stirling, and G. H. Lander, Phys. Rev. B **37**, 1846 (1988).
[31] S. I. Itoh, H. Ikeda, H. Yoshizawa, M. J. Harris, and U. Steigenberger, J. Phys. Soc. Jpn. **67**, 3610 (1998).
[32] S. H. Lee, J. M. Tranquada, K. Yamada, D. J. Buttrey, Q. Li, and S. W. Cheong, Phys. Rev. Lett. **88**, 126401 (2002).
[33] C. R. Anderson, K. H. Andersen, J. Bossy, W. G. Stirling, R. M.

Dimeo, P. E. Sokol, J. C. Cook, and D. W. Brown, Phys. Rev. B **59**, 13588 (1999).
[34] J. Saroun and J. Kulda, Physica B **234**, 1102 (1997).
[35] M. F. Collins, *Magnetic Critical Scattering* (OUP, USA, 1989).
[36] R. A. Cowley, W. J. L. Buyers, and G. Dolling, Solid State Commun. **7**, 181 (1969).
[37] G. Shirane and Y. Yamada, Phys. Rev. **177**, 858 (1969).
[38] K. Otnes, T. Riste, G. Shirane, and J. Feder, Solid State Commun. **9**, 1103 (1971).
[39] W. J. L. Buyers and T. M. Holden, *Handbook of the Physics and Chemistry of the Actinides* (North-Holland, Amsterdam, 1985), Vol. 2, p. 239.
[40] R. Caciuffo, G. Amoretti, P. Santini, G. H. Lander, J. Kulda, and P. de V. Du Plessis, Phys. Rev. B **59**, 13892 (1999).
[41] M. A. Ivanov, V. A. Kimasov, and Y. F. Markov, Phys. Solid State **44**, 373 (2002).
[42] W. D. Ellenson and J. K. Kjems, J. Chem. Phys. **67**, 3619 (1977).
[43] H. Cailleau, A. Girard, F. Moussa, and C. M. E. Zeyen, Solid State Commun. **29**, 259 (1979).